# A Unique Bridging Facet Assembly of Gold Nanorods for the Detection of Thiram through Surface-Enhanced Raman Scattering

Bhavya M. B.,[a] Ramya Prabhu B,[b] Sudesh Yadav,[c] Neena S. John,[b] Ali Altaee,[c] Manav Saxena,[a] Akshaya K. Samal[a]*

Bhavvya M. B.[a], Ramya Prabhu B.[b], Anjana Tripathi[c], Sudesh Yadav[d], Neena S. John[b], Ranjit Thapa[c], Ali Altaee[d], Manav Saxena[a], and Akshaya K. Samal[a*]

[a]Centre for Nano and Material Sciences, Jain University, Jain Global Campus, Ramanagara, Bangalore 562112, India

[b]Centre for Nano and Soft Matter Sciences, Jalahalli, Bangalore 560013, India

[c]Department of Physics, SRM University-AP, Amaravati 522240, Andhra Pradesh, India

[d]Centre for Green Technology, School of Civil and Environmental Engineering, University of Technology Sydney, 15 Broadway, NSW 2007, Australia

**Abstract**

Concerns have grown in recent years about the widespread use of the pesticide thiram (TRM), which has been linked to negative effects on local ecosystems. This highlights the critical need for quick and accurate point-of-need pesticide analysis tools for real-time applications. The detection TRM using gold nanorods (Au NRs) with a limit of detection (LOD) of $10^{-11}$ M (10 pM) and an enhancement factor (EF) of $2.8 \times 10^6$ was achieved along with good signal homogeneity of 6.2% (with respect to peak at 1378 $cm^{-1}$) calculated via surface-enhanced Raman scattering (SERS). Spectroscopic analysis reveals the formation of the Au-S bond, which emphasizes the adsorption of TRM on Au NRs through the Au-S bond. Addition of Au NRs to TRM of higher and lower concentration yields side-by-side assembly (SSA) and bridging facets assembly (BFA), respectively and exhibited excellent hotspots for the ultra-low detection of TRM. Bridging facets of Au NRs, such as (5 12 0) and (5 0 12) planes, are mainly responsible for the BFA. This kind of interaction is observed for the first time and not reported elsewhere. The detailed facets of Au NRs, namely side facets, bridging facets and pyramid facets, were discussed with the 3D model of Au NRs. The interaction of Au NRs with TRM is sensitive, and ultra-low detection of hazardous TRM

makes SERS an ideal technique for environmental protection, real-time applications and analysis of one-of-a-kind materials.

**Key-words**: Gold nanorods (Au NRs); Thiram (TRM), Surface-enhanced Raman scattering (SERS), Side by side assembly (SSA), and Bridging facets assembly (BFA)

## Introduction

Surface-enhanced Raman scattering (SERS) stands as an excellent technique for the ultra-low detection of hazardous substances responsible for environmental contamination.[1] SERS is a powerful technique due to its high sensitivity for detecting the ultra-low concentration of analyte with less acquisition and accumulation time compared to currently employed spectroscopic methods. Hence, this method is prominent and appropriate for analyte sensing at extreme ultra-low concentrations.[2,3] Among different environmentally hazardous substances, pesticides are one of the major contaminants[4] and detection of these hazardous substances is highly necessary.

In a substantial move, Pesticide Action Network (PAN) India welcomes the Government's proposal of banning 27 highly toxic pesticides in India on May 14$^{th}$, 2020.[5] These 27 pesticides are currently used in India and have been banned in different countries. The shocking revelation is that thiram (TRM) pesticide is one among them.[5] Earlier, TRM was classified as "not likely to be carcinogenic to humans" according to the Environmental Protection Agency (EPA) on July 2$^{nd}$, 1999.[6] But due to the non-standard and prolonged usage, it is banned in some countries now and but currently practised in India.[6] Because of its hazardous effects, detection of TRM is highly beneficial for living entities and the environment.

Many research groups have proposed a variety of complex substrates for TRM detection, with mixed results in substrate complexity, the limit of detection (LOD), and substance uniformity for TRM detection at ultra-low concentrations. Liu et al. used Ag@Au core-shell nanoparticles on polyimide to detect TRM. They achieved LOD up to $10^{-9}$ M.[7] TRM was detected at an LOD of $3.8 \times 10^{-9}$ M using Ag nanoparticle-decorated bacterial nanocellulose.[8] Our previous work achieved a LOD of 10 fM and 1 nM detection of TRM with Ag NCs and Ag NRs, respectively.[9]

Kim et al. used 2,2,6,6-tetramethylpiperidine-1-oxy-oxidized cellulose nanofibers (TEMPO-CNF) with Au NRs which achieved TRM detection up to $2.4 \times 10^{-8}$ M / $cm^2$.[10] Yu and co-workers prepared Au NR-coated capillaries as SERS substrate for TRM detection and achieved LOD of $9.98 \times 10^{-9}$ M /$cm^2$.[11] The comparison table (Table.1) is given below in result and discussion part. It comprises recent literature outlook for the different substrates employed, laser wavelength and LOD obtained for the TRM detection are compared with the present work. Here, the general morphologies, and particularly those to Au NRs, are tabulated separately. It is clearly observed that the present work yielded a LOD of $10^{-11}$ M (10 pM), a much lower value compared to other previously reported work with Au NRs as substrates.

The present work focuses on the detection of TRM using Au NRs through SERS. The addition of Au NRs to TRM resulted in side by side (SSA) and bridging facets assembly (BFA) with a higher and lower concentration of TRM, respectively. Many researchers have reported side by side and end to end interacted Au NRs with the addition of external additives such as dimercaptosuccinic acid (DMSA),[12] 3-mercaptopropionic acid (MPA), 11-mercaptoundecanoic acid (MUA),[13] DNA,[14] etc. which are helpful for the formation of assembly of Au NRs. In our previous work, we also reported the side by side and end to end interacted Au NRs upon adding chlorpyrifos and malthion pesticides, respectively.[4] But in the present work, we observed a unique kind of interaction or assembly, i.e., bridging facets interacted Au NRs with a lower concentration of TRM. This kind of interaction is briefly referred to as BFA, observed for the first time and not reported elsewhere. When adding Au NRs to the TRM, the NRs were self-assembled and excellent hotspots were generated at the nanogaps of Au NRs. The present work achieved a LOD of $10^{-11}$ M (10 pM), which is very much lesser than the permissible limit of 7 ppm ($2.9 \times 10^{-5}$ mol $L^{-1}$)[15] and an enhancement factor (EF) of $2.8 \times 10^6$. The cumulation of spectral intensities of 25 different random locations on the TRM-Au NRs sample yields excellent signal homogeneity, i.e., relative standard deviation (RSD) of 6.2% (with respect to peak at 1378 $cm^{-1}$). Because of lower LOD in less time, better EF and good signal homogeneity, Au NRs were demonstrated as potential substrates in TRM detection through the SERS technique.

**Materials and methods**

The details of the materials and methods are given in the supporting information.

**Experimental Section:**

Seed mediated method was employed for the synthesis of Au NRs, as reported elsewhere.[4,16] Two steps are involved in the synthesis of Au NRs, and a detailed experimental procedure is given in the supporting information.

**Results and discussion**

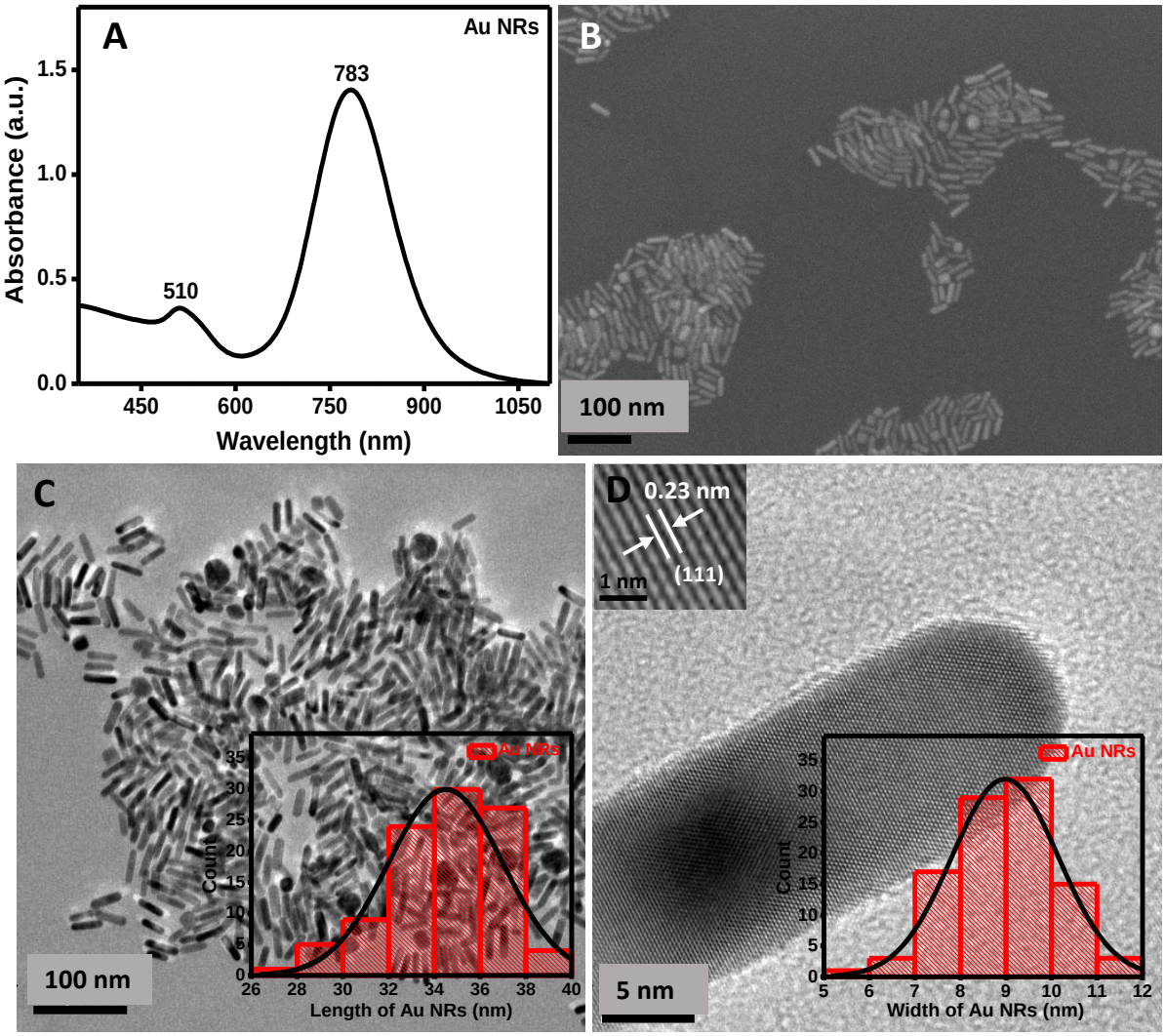


**Figure 1.** (A) UV-vis spectrum, (B) FESEM image of Au NRs, (C) TEM image, and (D) HRTEM image of Au NR. Inset of (C) and (D) shows the histograms corresponding to the length and breadth of Au NRs, respectively. One more inset of (D) shows the interplanar distance of the gold lattice.

UV-Vis absorption spectra were collected for synthesized Au NRs. They displayed two absorption peaks at 510 and 783 nm, corresponding to transverse surface plasmon (TSP) and longitudinal surface plasmon (LSP), respectively, as shown in Fig. 1A. The surface morphology of the synthesized nanostructure showed rod-like structures confirmed by FESEM analysis. In Fig. 1B, the length and breadth of Au NRs as assessed by FESEM analysis, are 35 ± 2 nm and 9 ± 2 nm, respectively, and the aspect ratio of Au NRs is 3.8 ± 0.2 nm.

TEM analysis was performed to authenticate further the synthesized morphology, which confirms the NR shape. A large area TEM of Au NRs is shown in Fig. 1C. The length and breadth of Au NRs obtained in TEM agree with the measurements obtained in FESEM. HRTEM analysis confirms the crystalline nature of Au NRs (Fig.1D) with 0.23 nm interplanar distance, which corresponds to (111) plane of Au, shown as an inset in Fig. 1D. Histograms are plotted for the length and width of Au NRs, where length and breadth vary from 35 ± 2 nm (inset Fig. 1C) and 9 ± 2 nm (inset Fig. 1D), respectively.

XRD analysis has been carried out to know the crystalline nature of Au NRs. Sharp peaks obtained from XRD confirm the crystalline nature of Au NRs and exhibit four major peaks of 2θ values at 38.2, 44.5, 64.67, and 77.7 correspond to (111), (200), (220) and (311), respectively as shown in Fig. S1A. Peaks obtained from XRD are in good agreement with the literature and are indexed to fcc of gold with JCPDS 00-001-1172.[17] The most intense peak obtained for the (111) plane suggests the growth of Au NRs along the (111) plane direction. SAED pattern is evident the different interplanar distances matched with the different planes of gold, namely the interplanar distances such as 0.23 nm, 0.20 nm, 0.14 nm, 0.12 nm, and 0.11 nm correspond to their planes of (111), (200), (220), (311), and (222), respectively as displayed in Fig. S1B.

To understand the detailed interaction, two different concentrations of TRM, 10 ppm and 200 ppm of 2 mL were taken individually in a glass vial and followed by 50 µL of purified Au NRs of intensity 1.4 each vial with stirring for 2 h 30 min. Then, the solution was centrifuged, and the obtained precipitate was used to study the interaction between Au NRs and TRM through various analyses. Initially, the TRM reacted Au NRs (TRM-Au NRs) was subjected to TEM analysis,

wherein 200 ppm of TRM with Au NRs formed a side to side assembly (SSA), and 10 ppm of TRM with Au NRs yields bridging facets assembly (BFA). Fig. 2A and 2B show the SSA and BFA of Au NRs with 200 ppm and 10 ppm of TRM, respectively. Elemental mapping analysis has been performed to know the extent of adsorption of TRM (200 ppm) on Au NRs, shown in Fig. 2C to 2F. Elemental mapping of Au shown in Fig. 2C and the adsorption of main elements of TRM such as S and N are displayed in Fig. 2D and Fig. 2E, respectively. Cumulative mapping of all the elements of TRM along with Au is shown in Fig. 2F. Elemental mapping is evident for the well and uniform adsorption of TRM over Au NRs.

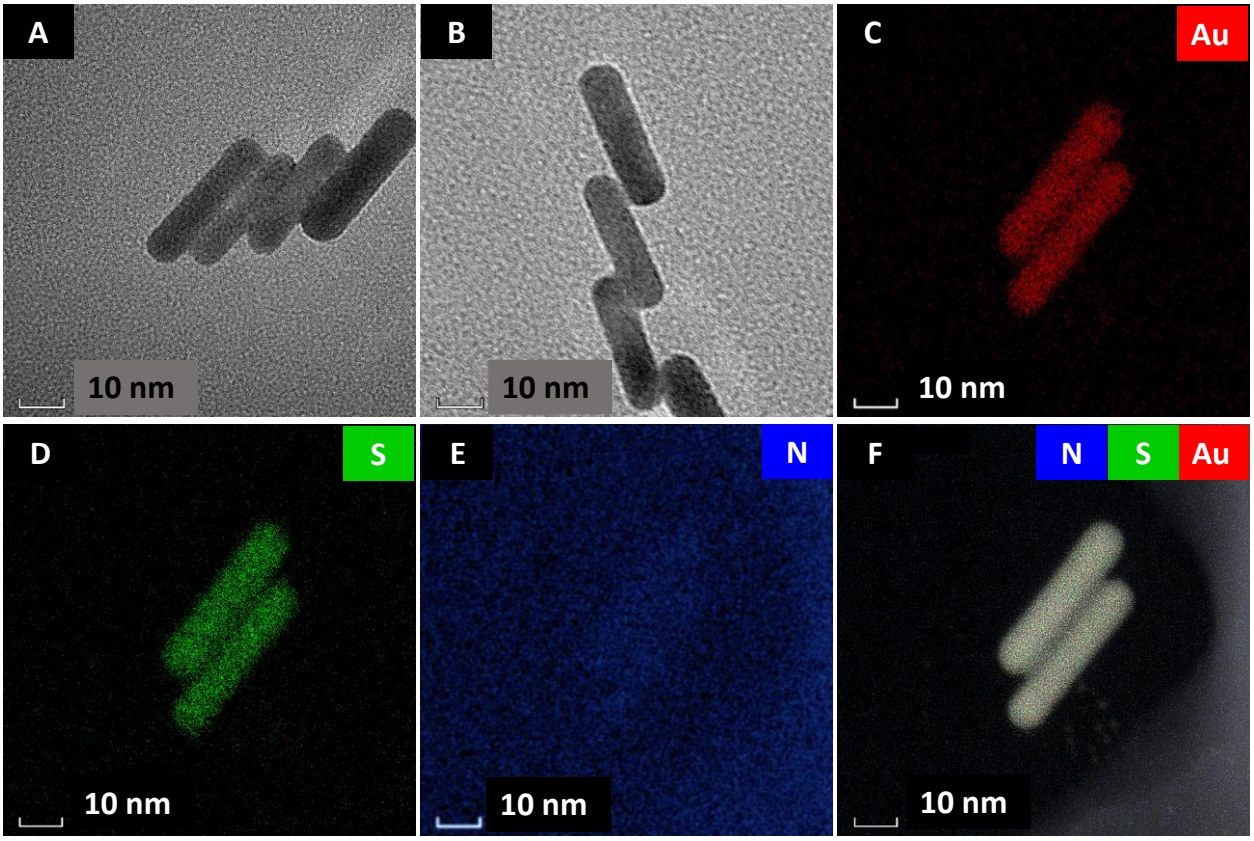


**Figure 2**. (A) and (B TEM images of TRM-Au NRs with TRM concentration of 200 and 10 ppm, respectively. (C) to (E) the individual elemental mapping of TRM-Au NRs and (F) the cumulative mapping of all the elements in TRM-Au NRs.

The line scan profile was carried out, enabling the analysis of a selected line on the cumulative mapping image as shown in Fig S2. The single selected line on the cumulative mapping image

observed in Fig S2A was 23 ± 0.2 nm for two side to side assembled Au NRs. The line scan shows the position (in nm) along the x-axis and integrated counts along the y-axis. Fig. S2B shows the line scan profile along the line in Fig. S2A and provides the information about the distribution of Au, S, and N over the selected line (23 ± 0.2 nm), which is strongly evident the adsorption of TRM over Au NRs. Energy-dispersive X-ray spectroscopy (EDS) analysis was performed, which further validate the well adsorption of TRM over Au NRs. Fig. S3 shows the EDS spectrum of TRM-Au NRs, where main elements of TRM such as S and N are presented along with Au.

FT-IR analysis was performed to determine the bonding interaction of TRM with Au NRs. Fig. S4 displayed the FT-IR analysis of Au NRs, TRM, and TRM-Au NRs. Fig. S4B is the magnified image of Fig. S4A in the region from 400 to 2000 $cm^{-1}$. All the bands observed in FT-IR spectra are in good agreement with the literature.[18,19] All the bands are detailed in Table 1 (SI) for TRM. CTAB capped Au NRs show the resolved bands at 2918 and 2850 $cm^{-1}$ are assigned to symmetric and asymmetric stretching of -$CH_2$- of CTAB chain, respectively.[20] Mainly, the band appeared at 563 $cm^{-1}$ attributed to stretching vibration of S-S and 441 $cm^{-1}$ assigned to C=S stretching vibration for TRM. After reacting with Au NRs, i.e. TRM-Au NRs, TRM clearly observed that the two bands at 441 and 563 cm-1 assigned to C=S and S-S, respectively, disappeared, as shown in Fig. S4B. This disappearance of two bands signposts that the S-S bond breaking and the S present in the C=S bond bind Au to form an Au-S bond due to the propensity of S to Au and evident by EDX, FT-IR and line profiles.

Raman analysis was carried out for bare TRM (1 mM) and TRM (1 µM)-Au NRs. The laser was normalized using three different wavelength lasers such as 532, 638 and 785 nm. Raman spectra of bare TRM at 1 mM shown in Fig. S5 and acquired with 638 nm laser was used with the laser power of 3 mW, accumulation of 2 cycles and acquisition time of 30 s. Laser normalization for TRM (1 µM)-Au NRs, shown in Fig. S6A. The laser normalization using three different lasers was plotted, and the comparative enhancement graph is given in Fig. S6B. The 638 nm laser provided higher intensity compared to the other two lasers and kept all the other parameters constant for all measurements. The detailed Raman and SERS spectral data are given in Table 1 (SI) and agree with the literature.[14] When TRM-Au NRs were subjected to Raman analysis, it is observed that intensities of some of the peaks varied, and the appearance of new peaks or disappearance of few

peaks provided strong evidence to explain the interaction between TRM and Au NRs. 1378 $cm^{-1}$ is the highest intensity and majorly changed peak in SERS, assigned to δ ($CH_3$) and υ (CN). The peak at 393 $cm^{-1}$, assigned to υ (C=S) (in the Raman spectra) was disappeared in SERS. This suggests that the S-S bond of TRM breaks, and the υ (C=S) and υ (C-S) peaks decrease with simultaneous enhancement in υ (CN) mode. Strong evidence for the chemical bonding of TRM through S with Au NRs is a new peak at 336 $cm^{-1}$ in SERS. This result strongly indicates the formation of the Au-S bond and is attributed to υ (Au-S) vibration.[21] Another new peak was observed at 1504 $cm^{-1}$ attributed to υ (C=N) weakly coupled with δ ($CH_3$). The appearance of this new peak was due to the formation of thioureide in the resonance structure of the TRM, which appeared after the bond formation with Au NRs.[21]

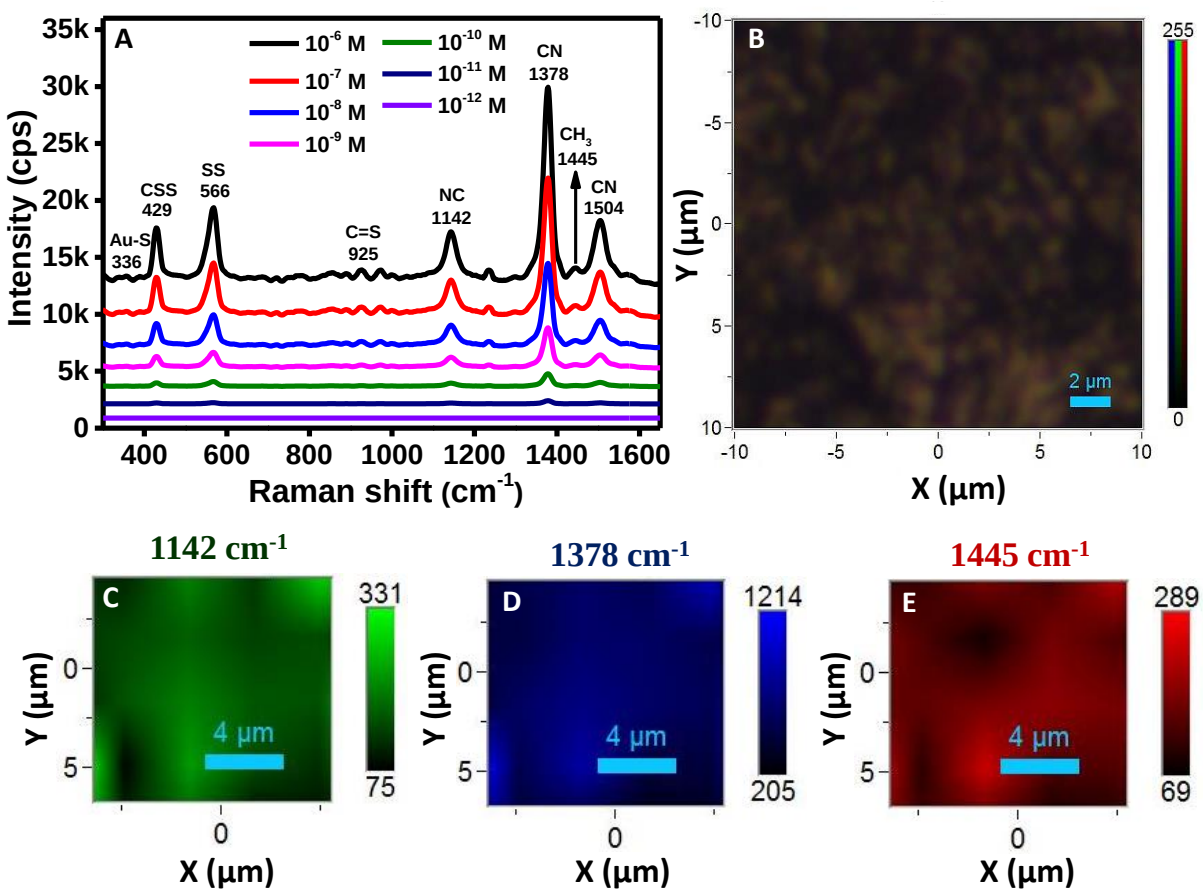


**Figure 3**. (A) SERS spectra of TRM-Au NRs with different concentrations of TRM varies from $10^{-6}$ to $10^{-12}$ M, (B) Optical image selected for Raman mapping of 10 × 10 μm area, (C)-(E) Raman

mapping images of three different peaks, 1142 $cm^{-1}$, 1378 $cm^{-1}$, 1445 $cm^{-1}$, represented in green, blue and red colour, respectively.

Further, SERS analysis was performed to know the limit of detection (LOD) of TRM with Au NRs. 638 nm laser was used with a laser power of 0.3 mW, accumulation of 2 cycles, and acquisition time of 30 s. SERS samples were prepared by drop casting 20 µL of TRM-Au NRs precipitate obtained after centrifugation on a glass slide. Samples were used for SERS analysis after drying of the sample in ambient conditions.

SERS analysis was carried out with different concentrations of TRM from $10^{-6}$ (1 µM) to $10^{-12}$ M (1 pM) with Au NRs. SERS spectra of TRM-Au NRs is shown in Fig. 3A. Individual spectra of TRM ($10^{-11}$ M)-Au NRs is clearly shown in Fig. S7. TRM was detected up to $10^{-11}$ M (10 pM); beyond this concentration, no characteristic peak of TRM was observed. Hence, 10 pM is the limit of detection (LOD). An optical image of 10 × 10 µm was selected for Raman mapping, shown in Fig. 3B.

Three peaks were selected for Raman mappings, such as 1142, 1378 and 1445 $cm^{-1}$, represented in green, blue and red colour, respectively shown in Fig. 3C to 3E. A 638 nm laser was used along with 3 mW laser power, accumulation of 2 cycles, and acquisition of 7 s as Raman mapping parameters. TRM (1 µM)-Au NRs was used for Raman mapping. Peaks were selected based on three different intensities, to brief, peaks at 1142, 1378 and 1445 $cm^{-1}$ were moderate, intense and weak in intensities, respectively, as shown in Fig. 3A. Acquisition time duration for Raman mapping (7 s) was set, which is less than SERS measurements (10 s), and hence, yielded with reduced peak intensities in Raman mapping compared to peak intensities shown in SERS (Fig. 3A). In Fig. 3C to E, a nearly uniform distribution of TRM can be seen for all three different peaks. Hence, from Raman mapping, it can be concluded that TRM was uniformly adsorbed over Au NRs. A plot of intensity versus concentration of different spectral positions such as 336 $cm^{-1}$, 429 $cm^{-1}$, 566 $cm^{-1}$, 925 $cm^{-1}$, 1142 $cm^{-1}$, 1378 $cm^{-1}$, 1445 $cm^{-1}$, and 1504 $cm^{-1}$ from SERS data with error bars is shown in Fig. 4A to H. The insets in Fig. 4A to H are the enlarged spectra of the same form $10^{-9}$ M to $10^{-12}$ M. This graph provided less deviation of intensities for all spectral positions.

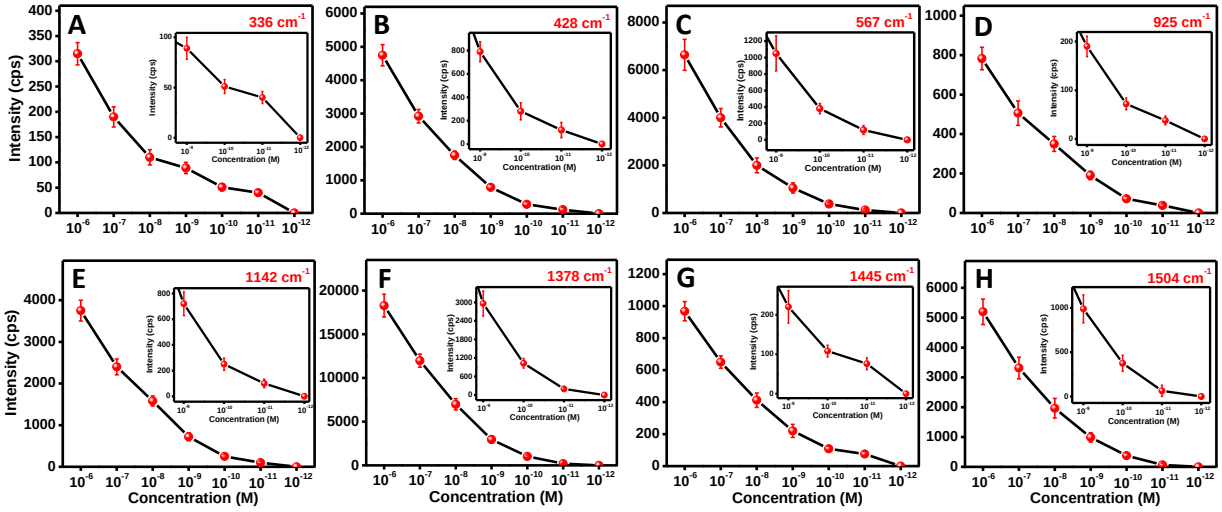


**Figure 4**: Plot of intensity versus concentration of different spectral position at (A) 336 $cm^{-1}$, (B) 429 $cm^{-1}$, (C) 566 $cm^{-1}$, (D) 925 $cm^{-1}$, (E) 1142 $cm^{-1}$, (F) 1378 $cm^{-1}$, (G) 1445 $cm^{-1}$, and (H) 1504 $cm^{-1}$.

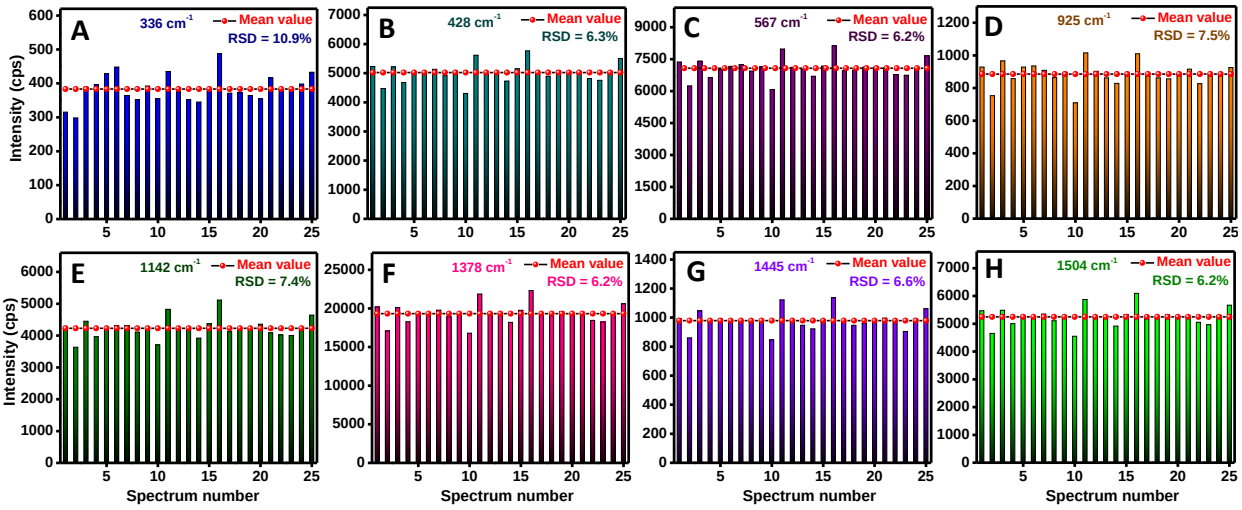


**Figure 5**: Plot of intensity versus spectrum number of TRM of 1 µM with Au NRs at (A) 336 $cm^{-1}$, (B) 429 $cm^{-1}$, (C) 566 $cm^{-1}$, (D) 925 $cm^{-1}$, (E) 1142 $cm^{-1}$, (F) 1378 $cm^{-1}$, (G) 1445 $cm^{-1}$, and (H) 1504 $cm^{-1}$.

A uniformity study was performed to identify the distribution of TRM over Au NRs, using 25 random spots on TRM (1 µM)-Au NRs and were plotted together as shown in Fig. S8. Here, in almost all spectra, the intensities were nearly comparable. Fig.5A to H show a plot of intensity versus spectrum number with respect to different spectral positions. All the spectral positions were shown with relative standard deviation (RSD) which can also be referred to signal homogeneity,

which are found ≤ 10 %, in particular, 336 $cm^{-1}$, 429 $cm^{-1}$, 566 $cm^{-1}$, 925 $cm^{-1}$, 1142 $cm^{-1}$, 1378 $cm^{-1}$, 1445 $cm^{-1}$, and 1504 $cm^{-1}$ provided with 10.9 %, 6.3 %, 6.2 %, 7.5 %, 7.4 %, 6.2 %, 6.6 % and 6.2 %, respectively. The lower RSD value shows that the values are not much deviated from the mean value.

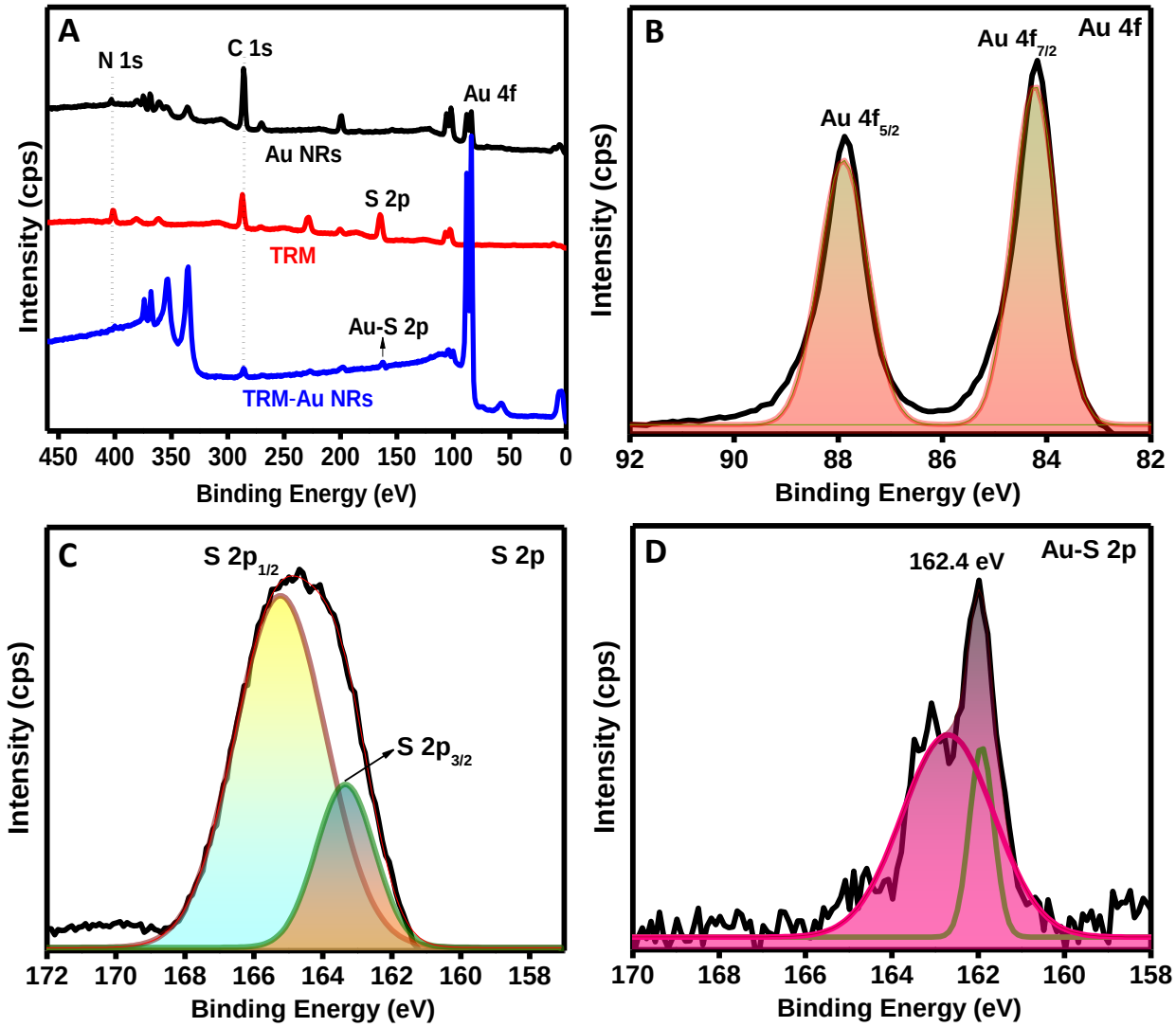


**Figure 6**: (A) XPS survey spectra of Au NRs, TRM, TRM-Au NRs, High resolution XPS spectra of (B) Au 4f, (C) S 2p, and (D) Au-S 2p.

X-ray photoelectron spectroscopy (XPS) analysis reveals the elemental composition of the samples. Fig. 6A shows the XPS survey spectra of Au NRs, TRM and TRM-Au NRs. All the spectral details for Au NRs, [22] TRM and TRM-Au NRs[23] are well-matched with the literature.

High-resolution spectra of Au 4f, S 2p and Au-S 2p were shown in Fig. 6B, C and D, respectively. Peaks at 84.1 eV and 87.8 eV corresponded to a doublet of Au $4f_{7/2}$ and $4f_{5/2}$, respectively and at 284.8 eV and 402.23 eV were attributed to C 1s and N 1s, respectively. S 2p peak appeared at 164.8 and 165.2 eV corresponds to S $2P_{3/2}$ and S $2P_{1/2}$, respectively. When Au NRs were added to the TRM solution, a new peak appeared at 162.6 eV, corresponding to Au-S 2p.[24] According to literature, the peak at 84.1 eV appears more significant due to the formation of the Au-S bond.[24,25] In the present work, we also observed an increase in the intensity of the peak at 84.1 eV. This is strong evidence for the formation of the Au-S bond.

The enhancement factor (EF) was calculated for bare TRM of 1 mM concentration and with TRM (1 µM)-Au NRs using equation 1.[26] 1 mM concentration of TRM was used to collect Raman spectra with a 638 nm laser of 1 mW laser power, two accumulation cycles with an acquisition time of 10 s, shown in Fig. S5 which provided a very low intensity of 59 counts. TRM (1 µM)-Au NRs sample with enhanced signal intensity with the same parameters used for bare TRM except with less laser power of 0.3 mW. The most intense peak in SERS observed at 1378 $cm^{-1}$ was considered for EF calculation. EF for TRM-Au NRs was calculated and found to be $2.8 \times 10^6$. The detailed EF calculation is shown in supporting information. The first step includes the ISERS/ I Raman calculation and the second step includes the EF calculation.

$$EF = \frac{I_{SERS}/C_{SERS}}{I_{Raman}/C_{Raman}} \ldots\ldots\ldots (1)$$

Where,

$I_{SERS}$ = Raman intensities of TRM molecules in the SERS sample (TRM-Au NRs)

$I_{Raman}$ = Raman intensities of bare TRM (1 mM),

$C_{SERS}$ = Concentration of TRM solution contributing to $I_{SERS}$

$C_{Raman}$ = Concentration of TRM solution contributing to $I_{Raman}$

**Table:1 Literature background of TRM detection with different substrates, wavelength of laser used and achieved LOD compared with present work.**

| Substrates | Laser (nm) | LOD | Reference |
|---|---|---|---|
| **General** | | | |
| Ag@Au core-shell nanoparticles on polyimide | 633 | $10^{-9}$ M | Ref. 7 |
| Ag nanoparticle-decorated bacterial nanocellulose | 532 | $3.8 \times 10^{-9}$ M | Ref. 8 |
| Ag nanocubes | 638 | $3.8 \times 10^{-15}$ M | Ref. 9 |
| Ag nanowires | 638 | $1 \times 10^{-9}$ M | Ref. 9 |
| **Au NRs** | | | |
| 2,2,6,6-tetramethylpiperidine-1-oxy-oxidized cellulose nanofibers with Au NRs | 785 | $2.4 \times 10^{-8}$ M / $cm^2$ | Ref. 10 |
| Au NR doped with $Fe_3O_4$ nanoparticles | 633 | $1 \times 10^{-9}$ M | Ref. 27 |
| Au NR-coated capillaries | 633 | $9.98 \times 10^{-9}$ M / $cm^2$ | Ref. 28 |
| Au NRs | 785 | $2 \times 10^{-9}$ M | Ref. 29 |
| Au NRs/poly (methyl methacrylate) membrane | 785 | $2 \times 10^{-9}$ M | Ref. 30 |
| Au NRs polymer metafilm | 633 | $1 \times 10^{-6}$ M | Ref. 31 |
| PDMS-assisted paper-based substrate of Au@Ag nanorods core-shell | 785 | $41.5 \times 10^{-8}$ M | Ref. 32 |
| **Au NRs** | **638** | **$10 \times 10^{-12}$ M** | **Present work** |

**Plausible mechanism of TRM-Au NRs interaction with facet dependent assembly of Au NRs**

The data obtained from FT-IR, Raman and XPS analyses confirm the formation of Au-S bonding. This is evident for the chemisorption of TRM on Au NRs, and the plausible mechanism is depicted and shown in Fig. 7. The addition of Au NRs to TRM results in breaking the S-S bond and forming a new Au-S bond through the S atom from CSS. In SERS, the appearance of a new peak at 336 $cm^{-1}$ attributed to the Au-S bond confirms the formation of the Au-S bond. The peak at 162.4 eV in the XPS spectrum also confirms the formation of the Au-S bond. Hence, it can be concluded that the disulfur (S-S) bond of TRM breaks with the addition and interaction with Au NRs, and the broken two sulfur atoms (attached to the C-N group) bind to Au NRs.

Theoretical studies, as well as models, have demonstrated the well-known morphology of Au NRs.[33,34] Current theories and models of growth mechanisms as well shape transformations[35] are supported by the conclusion that Au NRs, which are synthesized with the addition of silver ions, are looped by the same facets as present in the bulk gold, specifically, {1 0 0}, {1 1 0}, or {1 1 1} facets which are closely packed atomic planes.[36,37]

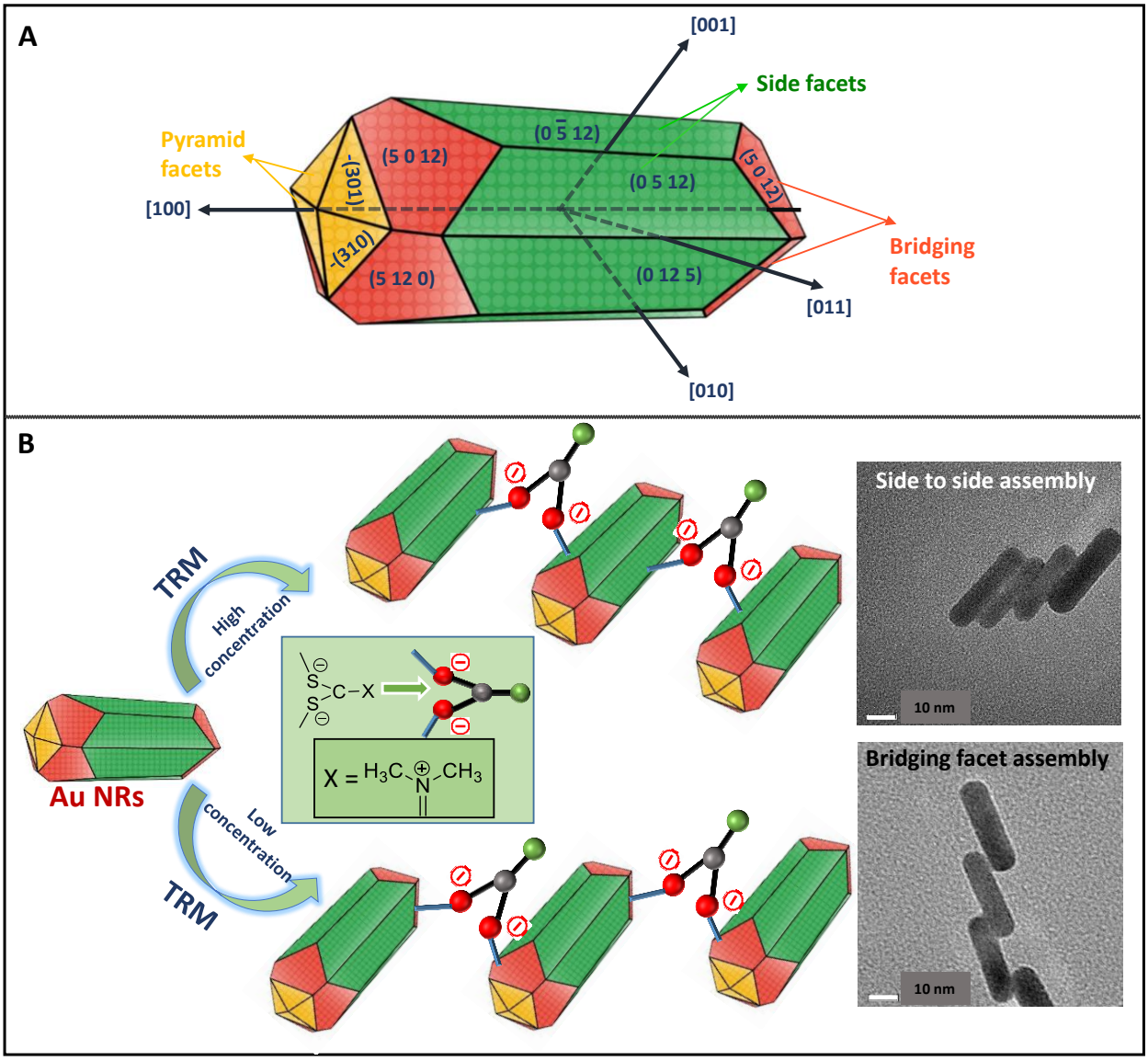


**Figure 7:** (A) 3D schematic representation of Au NRs representing three different types of facets, (B) Pictorial representation of plausible mechanism for higher lower and higher concentration of TRM with Au NRs.

Present morphological models emphasize the Au NRs as an octagon moulded by four {0 0 1} and four {0 1 1} side facets and ended by {1 0 0}, {1 1 0}, or {1 1 1} facets.[37] Basically, Au NRs have three types of facets: pyramid facets, side facets, and bridging facets which helps to connect side facets and end pyramid facets.[38] Fig. 6A represents the 3D schematic representation of Au NRs, representing all three types of facets. For the interaction study of Au NRs and TRM, Au NRs were added individually to 10 ppm and 200 ppm of TRM. The higher concentration of TRM leads to side-by-side assembly (SSA), and lower concentration leads to bridging facets assembly (BFA) of Au NRs. Inadequately packed (0 5 12) family of facets having a high index and are more reliable for the high affinity of the surfactants for the surface of gold.[38] The chemisorption reduces surface free energy, and further high-index facets were stabilized. This stabilization enables the adsorption of additional extra surfactant on the (0 5 12) facets.[38]

So, when Au NRs are added to a higher concentration of TRM, the TRM molecules preferably adsorb to (0 5 12). Meanwhile, when Au NRs are added to TRM of lower concentration, they prefer to bind to the facet, which is lower in CTAB concentration. TRM adsorbs to (5 0 12) facets and forms BFA. The reason for this kind of BFA may be due to the comparable compatibility of (5 0 12) plane for the lower concentration of TRM.

## Conclusion

To conclude, Au NRs were synthesized successfully using the seed-mediated method and characterized by UV-Vis analysis, SEM, TEM, FT-IR, Raman and XPS analysis. Synthesized Au NRs were employed for the detection of TRM. Upon adding Au NRs to TRM of higher and lower concentrations yields side by side (SSA) and bridging facet assembly (BFA), validated by TEM analysis. This unique BFA was observed for the first time and not reported before to the best of our knowledge. Elemental mapping confirms the good adsorption of TRM over Au NRs, and FT-IR, Raman, SERS, and XPS analysis confirm the adsorption of TRM on Au NRs through Au-S bond. A uniformity study was performed for the TRM-Au NRs sample using 25 random places and obtained an RSD of $\leq$ 10% for each peak in SERS. This shows TRM is uniformly adsorbed on Au NRs. LOD and EF were achieved at 10 pM and $2.8 \times 10^6$, respectively. Hence, Au NRs are considered as an excellent substrate in the detection of TRM. The unique assembly of BFA brings

more concern among the research community to further study the facet-dependent interactions of Au NRs.

**Acknowledgement**

BMB acknowledges JAIN University for Junior Research fellowship. AKS is grateful to the SERB, New Delhi, India for funding to conduct the research (CRG/2018/003533) and Karnataka Science and Technology Promotion Society (KSTePS/VGST-RGS-F/2018-19/GRD No.831/315). The authors acknowledge Nano Mission project (SR/NM/NS-20/2014) for FESEM facility. The authors thank Central Research Facility at CeNS for providing TEM and Confocal Raman microscope facility.

**Conflicts of interest**

There are no conflicts to declare.

**References**

1. Fu, Z.; Shen, Z.; Fan, Q.; Hao, S.; Wang, Y.; Liu, X.; Tong, X.; Kong, X.; Yang, Z., Preparation of multi-functional magnetic–plasmonic nanocomposite for adsorption and detection of thiram using SERS. *J. Hazard. Mater.* **2020,** *392*, 122356.

2. Abu Hatab, N. A.; Oran, J. M.; Sepaniak, M. J., Surface-enhanced Raman spectroscopy substrates created via electron beam lithography and nanotransfer printing. *ACS nano* **2008,** *2* (2), 377-385.

3. Chen, M.; Luo, W.; Liu, Q.; Hao, N.; Zhu, Y.; Liu, M.; Wang, L.; Yang, H.; Chen, X., Simultaneous in situ extraction and fabrication of surface-enhanced Raman scattering substrate for reliable detection of thiram residue. *Anal. Chem.* **2018,** *90* (22), 13647-13654.

4. MB, B.; Manippady, S. R.; Saxena, M.; John, N. S.; Balakrishna, R. G.; Samal, A. K., Gold nanorods as an efficient substrate for the detection and degradation of pesticides. *Langmuir* **2020,** *36* (26), 7332-7344.

5. PAN India response on the Draft Banning of Insecticides Order 2020 Date: 20.05.2020. Available at: https://pan-india.org/wp-content/uploads/2020/05/PAN-India_PR-_Draft-Pesticide-ban-order-21May2020.pdf.

6. United States Environmental Protection Agency, EPA 738-F-04-010 September 2004 – EPA R.E.D. Facts: Thiram. Available at: http://www.epa.gov/oppsrrd1/ REDs/factsheets/0122fact_thiram.pdf. Accessed 29 July 2014.

7. Liu, X.; Ma, J.; Jiang, P.; Shen, J.; Wang, R.; Wang, Y.; Tu, G., Large-scale flexible surface-enhanced Raman scattering (SERS) sensors with high stability and signal homogeneity. *ACS Appl. Mater. Interfaces* **2020,** *12* (40), 45332-45341.

8. Huo, D.; Chen, B.; Meng, G.; Huang, Z.; Li, M.; Lei, Y., Ag-nanoparticles@ bacterial nanocellulose as a 3D flexible and robust surface-enhanced Raman scattering substrate. *ACS ACS Appl. Mater. Interfaces* **2020,** *12* (45), 50713-50720.

9. Bhavya, M.; Shenoy, B. M.; Bhol, P.; Swain, S.; Saxena, M.; John, N. S.; Hegde, G.; Samal, A. K., Femtomolar detection of thiram via SERS using silver nanocubes as an efficient substrate. *Environ. Sci. Nano* **2020,** *7* (12), 3999-4009.

10. Kim, D.; Ko, Y.; Kwon, G.; Kim, U.-J.; Lee, J. H.; You, J., 2, 2, 6, 6-tetramethylpiperidine-1-oxy-oxidized cellulose nanofiber-based nanocomposite papers for facile in situ surface-enhanced Raman scattering detection. *ACS Sustain. Chem. Eng.* **2019,** *7* (18), 15640-15647.

11. Yu, Y.; Zeng, P.; Yang, C.; Gong, J.; Liang, R.; Ou, Q.; Zhang, S., Gold-nanorod-coated capillaries for the SERS-based detection of thiram. *ACS Appl. Nano Mater.* **2019,** *2* (1), 598-606.

12. Sreeprasad, T.; Samal, A.; Pradeep, T., One-, two-, and three-dimensional superstructures of gold nanorods induced by dimercaptosuccinic acid. *Langmuir* **2008,** *24* (9), 4589-4599.

13. Thomas, K. G.; Barazzouk, S.; Ipe, B. I.; Joseph, S. S.; Kamat, P. V., Uniaxial plasmon coupling through longitudinal self-assembly of gold nanorods. *J. Phys. Chem.* **2004,** *108* (35), 13066-13068.

14. Wang, G.; Akiyama, Y.; Kanayama, N.; Takarada, T.; Maeda, M., Directed Assembly of Gold Nanorods by Terminal-Base Pairing of Surface-Grafted DNA. *Small* **2017,** *13* (44), 1702137.

15. Dou, X.; Li, X.; Qin, L.; Han, S.; Kang, S.-Z., An ultrasensitive, disposable, and "plug and play" surface-enhanced raman scattering substrate for the in situ detection of trace thiram in water. *ACS Appl. Nano Mater.* **2018,** *1* (9), 4955-4963.

16. Sau, T. K.; Murphy, C. J. Seeded high yield synthesis of short Au nanorods in aqueous solution. *Langmuir* **2004,** *20*, 6414-6420.

17. Emam, A.; Mohamed, M.; Girgis, E.; Rao, K. V., Hybrid magnetic–plasmonic nanocomposite: embedding cobalt clusters in gold nanorods. *RSC Adv.* **2015,** *5* (44), 34696-34703.

18. J.-S. Kang, S.-Y. Hwang, C.-J. Lee and M.-S. Lee, *Bull. Korean Chem. Soc.* 2002, **23**, 1604-1610.

19. Seki, H., Raman spectra of molecules considered to be surface enhanced. Stud. Surf. Sci. Catal., Elsevier: 1983; Vol. 14, pp 287-297.

20. Su, G.; Yang, C.; Zhu, J.-J., Fabrication of gold nanorods with tunable longitudinal surface plasmon resonance peaks by reductive dopamine. *Langmuir* **2015,** *31* (2), 817-823.

21. Verma, A. K.; Soni, R., Silver nanodendrites for ultralow detection of thiram based on surface-enhanced Raman spectroscopy. *Nanotechnology* **2019,** *30* (38), 385502.

22. He, J.; Unser, S.; Bruzas, I.; Cary, R.; Shi, Z.; Mehra, R.; Aron, K.; Sagle, L., The facile removal of CTAB from the surface of gold nanorods. *Colloids Surf. B: Biointerfaces* **2018,** *163*, 140-145.

23. Bourg, M.-C.; Badia, A.; Lennox, R. B., Gold− sulfur bonding in 2D and 3D self-assembled monolayers: XPS characterization. *J. Phys. Chem.* **2000,** *104* (28), 6562-6567.

24. Brust, M.; Walker, M.; Bethell, D.; Schiffrin, D. J.; Whyman, R., Synthesis of thiol-derivatized gold nanoparticles in a two-phase liquid–liquid system. *Chem. Soc., Chem. commun.* **1994,** (7), 801-802.

25. McNeillie, A.; Brown, D. H.; Smith, W. E.; Gibson, M.; Watson, L., X-ray photoelectron spectra of some gold compounds. *J. Chem. Soc., Dalton Trans.* **1980,** (5), 767-770.

26. Khlebtsov, B. N.; Khanadeev, V. A.; Panfilova, E. V.; Bratashov, D. N.; Khlebtsov, N. G., Gold nanoisland films as reproducible SERS substrates for highly sensitive detection of fungicides. *ACS Appl. Mater. Interfaces* **2015,** *7* (12), 6518-6529.

27. Tang, S.; Li, Y.; Huang, H.; Li, P.; Guo, Z.; Luo, Q.; Wang, Z.; Chu, P. K.; Li, J.; Yu, X.-F., Efficient enrichment and self-assembly of hybrid nanoparticles into removable and magnetic SERS substrates for sensitive detection of environmental pollutants. *ACS Appl. Mater. Interfaces* **2017,** *9* (8), 7472-7480.

28. Yu, Y.; Zeng, P.; Yang, C.; Gong, J.; Liang, R.; Ou, Q.; Zhang, S., Gold-nanorod-coated capillaries for the SERS-based detection of thiram. *ACS Appl. Nano Mater.* **2019,** *2* (1), 598-606.

29. Li, X.; Lin, X.; Lin, S.; Zhou, S.; Fang, G.; Zhao, H.; Wang, L.; Cong, S., From Dilute to Multiple Layers: Bottom-Up Self-Assembly of Rough Gold Nanorods as SERS Platform for Quantitative Detection of Thiram in Soil. *Adv. Mater. Interfaces* **2021**, 2100412.

30. Yang, N.; You, T.-T.; Gao, Y.-K.; Zhang, C.-M.; Yin, P.-G., Rapid fabrication of flexible and transparent gold nanorods/poly (methyl methacrylate) membrane substrate for SERS nanosensor application. *Acta A Mol. Biomol. Spectrosc.* **2018,** *202*, 376-381.

31. Yang, N.; You, T.-T.; Gao, Y.-K.; Zhang, C.-M.; Yin, P.-G., Fabrication of a flexible gold nanorod polymer metafilm via a phase transfer method as a SERS substrate for detecting food contaminants. *J. Agric. Food Chem.* **2018,** *66* (26), 6889-6896.

32. Lin, S.; Hasi, W.; Han, S.; Lin, X.; Wang, L., A dual-functional PDMS-assisted paper-based SERS platform for the reliable detection of thiram residue both on fruit surfaces and in juice. *Anal. Methods* **2020,** *12* (20), 2571-2579.

33. Barnard, A. S.; Curtiss, L. A., Modeling the preferred shape, orientation and aspect ratio of gold nanorods. *J. Mater. Chem. A* **2007,** *17* (31), 3315-3323.

34. Lofton, C.; Sigmund, W., Mechanisms controlling crystal habits of gold and silver colloids. *Adv. Funct. Mater.* **2005,** *15* (7), 1197-1208.

35. Carbó-Argibay, E.; Rodríguez-González, B.; Pacifico, J.; Pastoriza-Santos, I.; Pérez-Juste, J.; Liz-Marzán, L. M., Chemical sharpening of gold nanorods: the rod-to-octahedron transition. *Angew. Chem. Int. Ed.* **2007,** *46* (47), 8983-8987.

36. Wang, Z.; Mohamed, M.; Link, S.; El-Sayed, M., Crystallographic facets and shapes of gold nanorods of different aspect ratios. *Surf. Sci.* **1999,** *440* (1-2), L809-L814.

37. Keul, H. A.; Möller, M.; Bockstaller, M. R., Structural evolution of gold nanorods during controlled secondary growth. *Langmuir* **2007,** *23* (20), 10307-10315.38.

38. Katz-Boon, H.; Rossouw, C. J.; Weyland, M.; Funston, A. M.; Mulvaney, P.; Etheridge, J., Three-dimensional morphology and crystallography of gold nanorods. *Nano lett.* **2011,** *11* (1), 273-278.

**TOC**

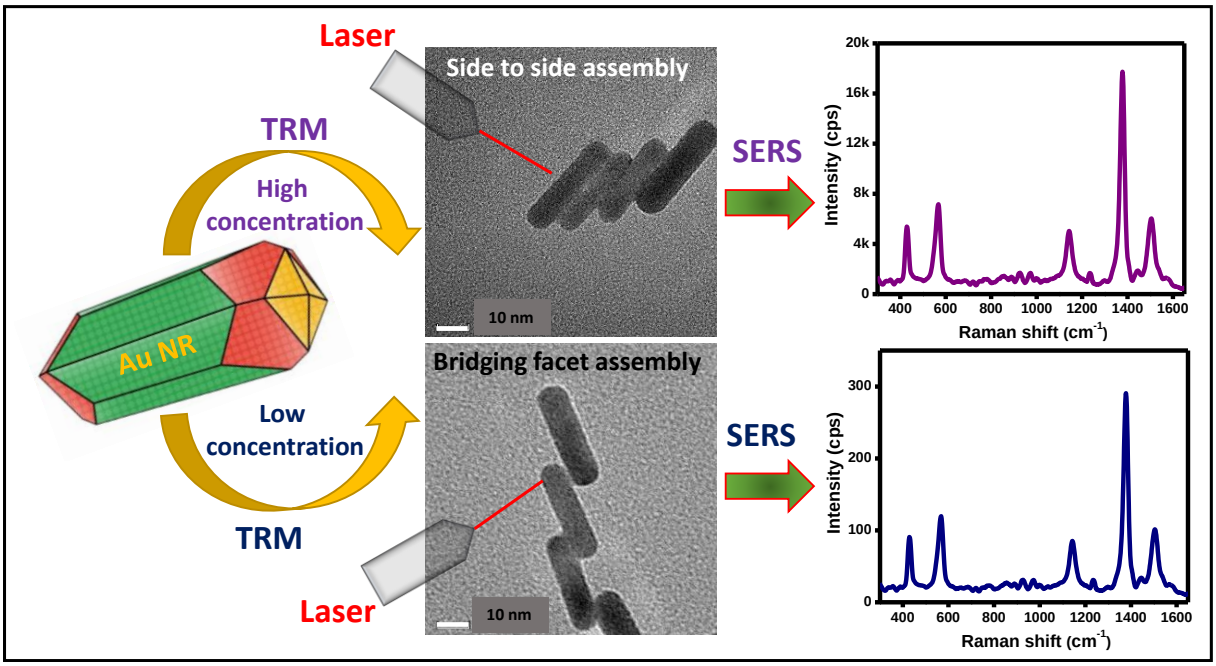
Laser
TRM
High concentration
Au NR
Low concentration
TRM
Laser
Side to side assembly
10 nm
Bridging facet assembly
10 nm
SERS
SERS
Intensity (cps)
Raman shift (cm-1)
Intensity (cps)
Raman shift (cm-1)